Structure of a bacterial pyridoxal 5′-phosphate synthase complex

Marco Strohmeier*, Thomas Raschle†, Jacek Mazurkiewicz‡, Karsten Rippe‡, Irmgard Sinning*, Teresa B. Fitzpatrick†§, and Ivo Tews*§

*Heidelberg University Biochemistry Center, Im Neuenheimer Feld 328, D-69120 Heidelberg, Germany; †ETH Zurich, Institute of Plant Sciences, Universitätstrasse 2, 8092 Zurich, Switzerland; and ‡Molecular Biophysics Group, Kirchhoff Institute for Physics, Heidelberg University, Im Neuenheimer Feld 227, D-69120 Heidelberg, Germany

Edited by Robert M. Stroud, University of California, San Francisco, CA, and approved October 14, 2006 (received for review June 15, 2006)

Vitamin B_6 is an essential metabolic cofactor that has more functions in humans than any other single nutrient. Its *de novo* biosynthesis occurs through two mutually exclusive pathways that are absent in animals. The predominant pathway found in most prokaryotes, fungi, and plants has only recently been discovered. It is distinguished by a glutamine amidotransferase, which is remarkable in that it alone can synthesize the cofactor form, pyridoxal 5′-phosphate (PLP), directly from a triose and a pentose saccharide and glutamine. Here we report the 3D structure of the PLP synthase complex with substrate glutamine bound as well as those of the individual synthase and glutaminase subunits Pdx1 and Pdx2, respectively. The complex is made up of 24 protein units assembled like a cogwheel, a dodecameric Pdx1 to which 12 Pdx2 subunits attach. In contrast to the architecture of previously determined glutamine amidotransferases, macromolecular assembly is directed by an N-terminal α-helix on the synthase. Interaction with the synthase subunit leads to glutaminase activation, resulting in formation of an oxyanion hole, a prerequisite for catalysis. Mutagenesis permitted identification of the remote glutaminase and synthase catalytic centers and led us to propose a mechanism whereby ammonia shuttles between these active sites through a methionine-rich hydrophobic tunnel.

3D structure | ammonia tunnel | glutamine amidotransferase | oxyanion | vitamin B_6

The term vitamin B_6 refers to the compounds pyridoxal, pyridoxine, pyridoxamine, and their phosphorylated derivatives. The vitamin is required for the catalytic function of numerous metabolic enzymes as well as for the upkeep of the nervous and immune systems in animals and has also recently been shown to be a potent antioxidant (1, 2). Two mutually exclusive *de novo* pathways exist, referred to as deoxyxylulose 5-phosphate (DXP)-dependent and DXP-independent (3). The DXP-dependent pathway is well characterized (4, 5), involving six proteins that catalyze the formation of pyridoxine 5′-phosphate, but is found only in a small subset of the γ-division of eubacteria (6). The DXP-independent pathway is much more predominant, being found in archaea, most eubacteria, fungi, apicomplexa, plants, and even some metazoans, but is less well characterized (2, 6, 7). The pathway is distinguished by the involvement of a glutamine amidotransferase (GATase), known as pyridoxal 5′-phosphate (PLP) synthase (8, 9).

GATases play a central role in metabolism, because they are responsible for the incorporation of nitrogen into amino acids, amino sugars, purine and pyrimidine nucleotides, coenzymes, and antibiotics (10). In general, they consist of a glutaminase domain where glutamine is hydrolyzed, yielding ammonia for use in a subsequent reaction specific for each GATase by the so-called synthase domain. The synthase subunit of PLP synthase, Pdx1, directly synthesizes PLP from either of the pentose sugars, ribose 5-phosphate or ribulose 5-phosphate, and either of the triose sugars, glyceraldehyde 3-phosphate or dihydroxyacetone phosphate, in the presence of the glutaminase subunit Pdx2 and glutamine. Although this pathway is of fundamental importance, its absence from animals may have implications for the discovery of new therapeutic agents (11), and it would greatly benefit from knowledge of the architecture of the enzyme complex. Recently, the 3D structures of the individual Pdx1 (12) and Pdx2 (13, 14) subunits have become available. Based on these structures, two independent hypotheses for the assembled PLP synthase have been proposed. One model (13) proposes an architecture akin to that of imidazole glycerol phosphate synthase (ImGP; refs. 15 and 16), where the synthase and glutaminase active sites are remote from each other. Implicit in this model is that there is a tunnel to channel the nascent ammonia between the disparate active sites. The second model (12) was proposed based on the structure of autonomous Pdx1 from *Geobacillus stearothermophilus* (named PdxS), where evidence for an ammonia tunnel could not be identified; thus, adjacent glutaminase and synthase active sites were predicted. In this work, we report the structure of the PLP synthase complex, in addition to those of the autonomous enzymes from *Bacillus subtilis*. This knowledge, in combination with biochemical and biophysical approaches, allows us to provide insight into the complicated mode of regulation and catalysis by an enzyme complex that synthesizes one of nature's most versatile cofactors.

Results

3D Structure of PLP Synthase. The determination of the 3D structure of PLP synthase necessitates stabilization of the enzyme complex, because the interaction of Pdx1 and Pdx2 is believed to be transient in nature (9), complicating its analysis. Pdx2 is a class I glutaminase categorized by the catalytic triad Cys-79, His-170, and Glu-172 (10). During studies probing the catalytic site, we introduced an H170N mutation (17) into *B. subtilis* Pdx2 (previously designated YaaE), which resulted in glutaminase activity indistinguishable from the background hydrolysis (Fig. 1*a Left*) with a concomitant loss in Pdx1 (previously designated YaaD) PLP synthesis activity (Fig. 1*a Right*). A native PAGE mobility-shift assay as described in ref. 9 was used to probe the nature of the Pdx1:Pdx2 complex in the presence of glutamine (Fig. 1*b Lower*). In this assay, the formation of the PLP synthase complex can be observed by a decrease in the mobility of Pdx1 (i.e., a mobility shift) due to its interaction with Pdx2. Moreover, Pdx2 can be immunodetected (9) in the shifted band of

Author contributions: M.S. and T.R. contributed equally to this work; K.R., T.B.F., and I.T. designed research; M.S., T.R., J.M., T.B.F., and I.T. performed research; M.S., T.R., J.M., K.R., I.S., T.B.F., and I.T. analyzed data; and I.S., T.B.F., and I.T. wrote the paper.

The authors declare no conflict of interest.

This article is a PNAS direct submission.

Abbreviations: GATase, glutamine amidotransferase; ImGP, imidazole glycerol phosphate synthase; PLP, pyridoxal 5′-phosphate.

Data deposition: The coordinates and structure factors have been deposited in the Protein Data Bank, www.pdb.org (PDB ID codes 2NV0, 2NV1, and 2NV2).

§To whom correspondence may be addressed. E-mail: tfitzpatrick@ethz.ch or ivo.tews@bzh.uni-heidelberg.de.

This article contains supporting information online at www.pnas.org/cgi/content/full/0604950103/DC1.

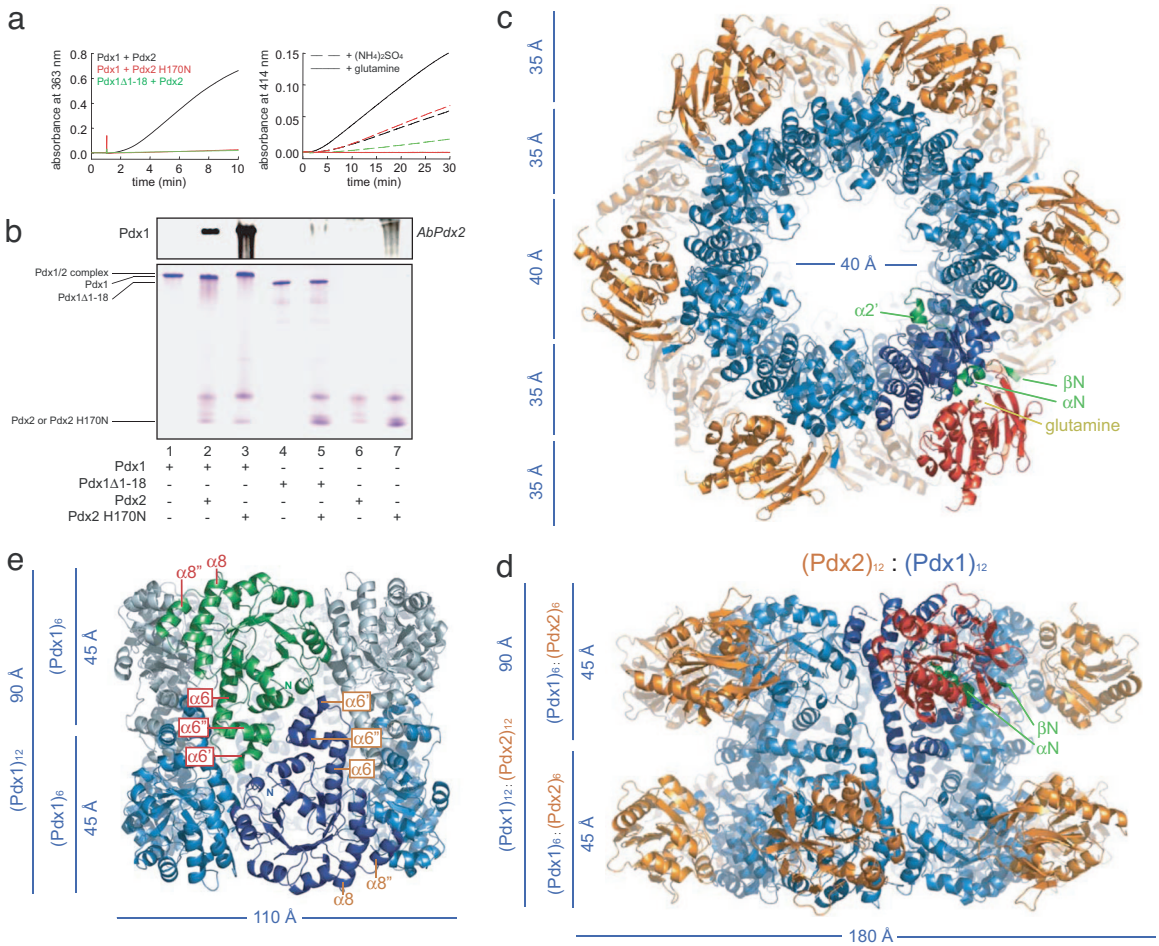

Fig. 1. Analysis of the *B. subtilis* Pdx1:Pdx2 H170N:glutamine ternary complex and autonomous Pdx1. (*a Left*) Glutaminase activity of Pdx2 WT (black), Pdx2 H170N (red) in the presence of Pdx1 WT, and Pdx2 WT in the presence of Pdx1 Δ1–18 (green). (*Right*) PLP synthase activity of Pdx1 in the presence of Pdx2 WT (black) or Pdx2 H170N (red) and of Pdx1 Δ1–18 in the presence of Pdx2 WT (green), using glutamine (solid lines) or ammonium sulfate (dashed lines) as the nitrogen source. (*b*) Analysis of complex formation by native PAGE (9). (*Lower*) Coomassie blue staining. Lane 1, Pdx1; lane 2, Pdx1 and Pdx2, lane 3, Pdx1 and Pdx2 H170N; lane 4, Pdx1 Δ1–18; lane 5, Pdx1 Δ1–18 and Pdx2 H170N; lane 6, Pdx2 WT; lane 7, Pdx2 H170N. (*Upper*) Western blot. The region of the gel where Pdx1 migrates was probed using a Pdx2-specific antibody (9). Glutamine (10 mM) was present in every case, and 10 pmol of each protein was loaded per lane. (*c* and *d*) The Pdx1:Pdx2 H170N:glutamine ternary complex shown in two orientations turned by 90°. Twelve Pdx2 glutaminase subunits attach to a double-ring-like core formed by 12 Pdx1 subunits. The Pdx1 synthase subunits are colored blue and green, and the Pdx2 glutaminase subunits are in orange and red. A single heterodimer is highlighted in dark blue (Pdx1) and red (Pdx2), and the position of bound glutamine is shown in stick representation. The N-terminal β-strand, βN, and α-helix, αN, as well as helix $\alpha 2'$ are highlighted in green. Approximate sizes are given in angstroms (10^{-10} m). (*e*) In the structure of the autonomous synthase subunit, Pdx1, the dodecameric assembly of protein subunits is identical to that in the ternary complex but lacking the N-terminal β-strand, βN, as well as helix $\alpha 2'$. Two hexameric rings lie on top of each other (pastel and light blue) and are interconnected by helices $\alpha 6$, $\alpha 6'$, and $\alpha 6''$ that point into dents of the adjacent ring. Two monomers are highlighted in green and blue in each ring.

Pdx1 (Fig. 1*b Upper*). Although Pdx2 interacts with Pdx1 using wild-type proteins (lane 2), immunodetection revealed a much higher presence of Pdx2 when mutant protein Pdx2 H170N is used (lane 3). A pronounced mobility shift is observed in the native PAGE (compare lanes 1 and 3), with a concurrent loss in the intensity of Pdx2 alone (compare lanes 7 and 3). These features indicated the assembly of a saturatable complex between Pdx1 and Pdx2 H170N and set the stage for crystallization trials of the enzyme complex.

The structure of the Pdx1:Pdx2 H170N:glutamine ternary complex has been determined at 2.1-Å resolution [R_{work} 15.4%, R_{free} = 20.5%; see supporting information (SI) Table 2]. The current refined structure contains a total of 5,568 amino acids or 42,000 atoms. Twelve Pdx1 synthase subunits form a double hexameric ring, to which 12 Pdx2 glutaminase subunits attach like the cogs of a cogwheel, interacting only with the Pdx1 subunits but not with each other (Fig. 1 *c* and *d*; a scheme depicting the complex assembly is shown in SI Fig. 5). The core of the complex, made up of Pdx1, is essentially unchanged from the structure of the autonomous protein (Fig. 1*e*), also determined at 2.1-Å resolution (R_{work} 14.4%; R_{free} 19.4%; see SI Table 2). Pdx1 folds as a $(\beta\alpha)_8$-barrel (18), whose axis is oriented nearly perpendicular to the ring perimeter. A bulge created by the helix $\alpha 8''$ at the C terminus running parallel to helix $\alpha 8$ establishes the contact between adjacent $(\beta\alpha)_8$-barrels. The hexameric rings interdigitate in the dodecameric structure. This is accomplished by elongation of helix $\alpha 6$ followed by two inserted helices $\alpha 6'$ and $\alpha 6''$, which protrude from the N-terminal face of each barrel on one hexameric ring into a corresponding dent in the other (Fig. 1*e*). We used analytical ultracentrifugation to assess PLP synthase in solution. The molecular masses were determined from the sedimentation velocity data by computing the molar mass distribution c(M) (19, 20). On its own, Pdx1 is present as two species with molecular masses of 186 ± 8 and 370 ± 11 kDa, corresponding to the hexameric and dodecameric forms, respectively (Table 1 and SI Fig. 6*a*, dotted line). The observed behavior is similar to the one described for PdxS (12). The data indicate that the dodecamer is the dominant species in solution (K_D = 3.7 μM; SI Fig. 6*c*). When Pdx1 was coexpressed and copurified with Pdx2 H170N, followed by gel

Table 1. Comparison of measured/calculated sedimentation coefficients

Species	S_{exp}, S*	S_{calc}, S†	M_{exp}, kDa‡	M_{calc}, kDa§	f/f_o¶
$(Pdx1)_6$	8.7 ± 0.3	8.1	186 ± 8	189.7	1.63
$(Pdx1)_{12}$	13.7 ± 0.3	13.9	370 ± 11	379.0	1.29
$(Pdx1)_{12}$-$(Pdx2)_{12}$‖	17.2 ± 0.8	18.6	576 ± 20	636.7	1.38

*The sedimentation coefficient determined under standard conditions (20°C, H_2O) from the c(s) distribution by using SEDFIT (19). Standard deviations were determined by averaging results from single fits.

†Calculated sedimentation coefficients using HYDROPRO and 3.3-Å bead size (35).

‡Molecular mass derived from molar mass distributions c(M).

§Calculated molecular mass.

¶Ratio of the friction coefficient (f) to the friction coefficient (f_o) of a sphere.

‖Pdx1:Pdx2 H170N in the presence of glutamine.

filtration in the presence of glutamine, only one species is observed by analytical ultracentrifugation (SI Fig. 6*a*, dashed line). The molecular mass corresponds to 576 ± 20 kDa and approximates that of a fully occupied Pdx1 dodecameric complex, i.e., with 12 monomers of Pdx2 attached (calculated mass, 636.7 kDa). The same result is obtained when the proteins are purified separately and then mixed in presence of glutamine (SI Fig. 6*b*, dashed line).

Structural Changes in the Pdx1 Synthase Subunit upon Complex Formation. The comparison of autonomous Pdx1 and the ternary complex highlights structural changes that occur upon complex assembly, namely formation of an extra N-terminal β-strand βN, an ordering of the N-terminal α-helix αN, and formation of an extra α-helix $\alpha2'$ (Figs. 1 and 2). The N terminus (residues 2–6) is involved in β-completion with $\beta7/\beta8$ of Pdx2 (Fig. 2). αN after β-strand βN is present in both the ternary complex and the structure of autonomous Pdx1, in contrast to the structure of PdxS (12), where it is absent. In autonomous Pdx1, αN (residues 7–17) has above-average B values, and a number of side chains are disordered. In the ternary complex, however, it is at the center of the interface and is well ordered. Importantly, αN covers the glutaminase active site and is held in place by two areas of polar interaction at either end of this helix, separated by a hydrophobic patch. One polar contact involves the side chain of Arg-8, which becomes ordered to interact with Glu-117 on $\beta7$ in Pdx2. Glu-117 also interacts with the side-chain hydroxyl of Thr-6 in Pdx1 (Fig. 2*b*). The second polar contact involves Lys-18 of Pdx1, which forms a salt bridge to Glu-15 in Pdx2. These two interactions allow for the precise alignment of αN, whereas the side chains of Met-13 and -16 in Pdx1 form an ordered hydrophobic interface with Ile-134 of Pdx2. In the structure of autonomous Pdx1, Arg-8, Met-13, Glu-15, and Met-16 are disordered, and Gln-17 and Lys-18 are in a different orientation. The side chain of Tyr-100 in the turn between $\alpha3$ and $\beta4$ points toward the Met-13/Ala-14 peptide bond in the autonomous Pdx1, whereas in the complex, it forms a hydrogen bond with the carbonyl oxygen of Lys-10 (Fig. 2*c*). The functional implication of reorienting Gln-17 and Tyr-100 is discussed below in light of the proposed mechanism for the transport of ammonia between the remote catalytic sites.

αN, not present in any of the other six class I GATase structures determined to date (21), is instrumental for complex formation. To corroborate its importance, we constructed a deletion mutant of Pdx1 missing the first 18 amino acids, Pdx1 Δ1–18. We then performed sedimentation velocity ultracentrifugation with Pdx1 Δ1–18 and found it does not interact with Pdx2 H170N in the presence of glutamine (SI Fig. 6*b*, dotted line), whereas native Pdx1 does (SI Fig. 6*b*, dashed line). Furthermore, native PAGE analysis of complex formation with Pdx2 H170N, as described above with the Pdx1 WT protein, indicated that Pdx1 Δ1–18 could not interact

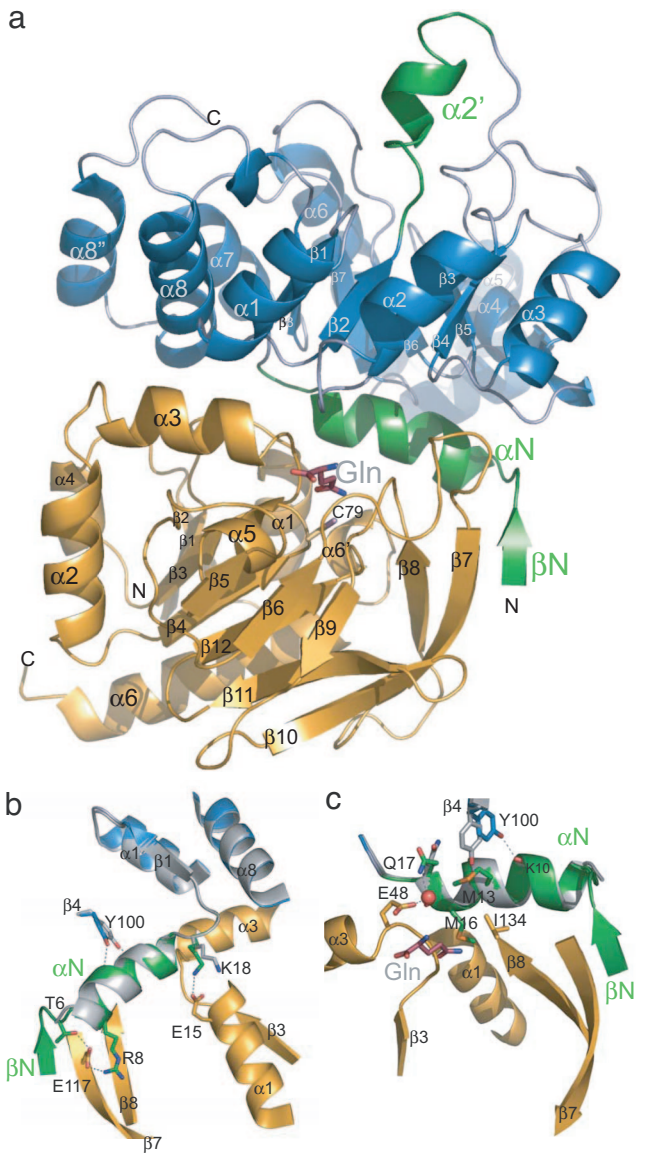

Fig. 2. Three major elements become ordered in Pdx1 (blue) upon complex formation with Pdx2 (orange). These are β-strand βN and helix $\alpha2'$ that form only in the complex as well as α-helix αN (all highlighted in green). (*a*) αN covers the glutaminase active site, whereas β-strand βN is involved in β completion with β-sheet $\beta7/\beta8$ of Pdx2. The Pdx2 substrate, glutamine, is shown in stick representation, as is the catalytic residue Cys-79 of Pdx2. (*b*) A comparison with the structure of autonomous Pdx1 (gray) highlights how residues of Pdx1 are ordered and reoriented on complex formation. αN is held in place by hydrogen-bonding networks around side chains Thr-6 and Arg-8 on one side and Lys-18 on the other. (*c*) View as in *b* but rotated by ≈180° around the vertical axis, with bound glutamine. The three amino acid side chains of Arg-8, Met-13, and Met-16 become ordered in the complex, whereas Tyr-100 and Gln-17 reorient.

with Pdx2 (Fig. 1*b*, lane 5). The Pdx1 Δ1–18 mutant was neither able to activate the glutaminase activity of Pdx2 (Fig. 1*a Left*) nor synthesize PLP in the presence of Pdx2 and glutamine (Fig. 1*a Right*). However, PLP synthesis was observed if ammonium sulfate was used as the nitrogen source (9), indicating an intact synthase domain (Fig. 1*a Right*).

Activation of the Glutaminase Subunit. Because the glutaminase activity of Pdx2 strictly depends on Pdx1 (9), a comparison of the Pdx1:Pdx2:glutamine ternary complex with the autonomous Pdx2 structure can be used to explain glutaminase activation. Pdx2 is a

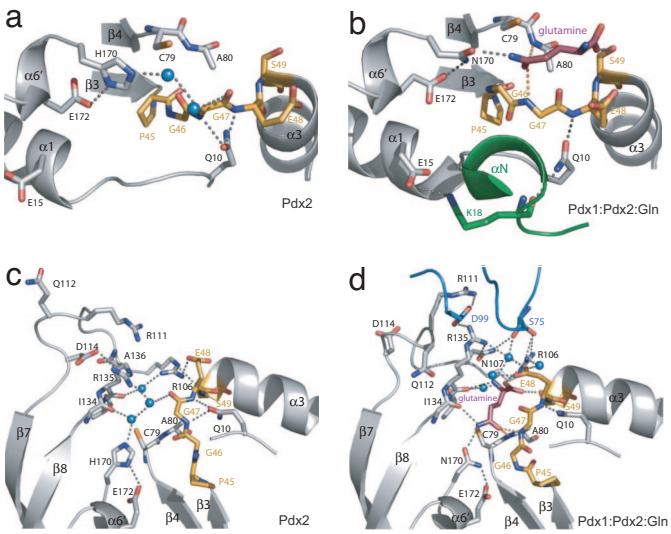

Fig. 3. Activation of glutaminase subunit by a peptide flip in the oxyanion region (ochre). (*a*) Glutaminase active site in the structure of autonomous Pdx2 showing the catalytic triad, Cys-79, His-170, and Glu-172. Peptide Gly-46–Gly-47 is not poised for catalysis, because the carbonyl of Gly-46 points toward the glutamine-binding site, stabilized by the hydrogen-bonding network involving Gln-10. (*b*) In the ternary complex with bound glutamine, however, Gly-46–Gly-47 has undergone a peptide flip, such that the oxyanion hole is now in place (orange dotted lines). The peptide is fixed in position by hydrogen-bonding contacts with Gln-10, which is stabilized by Lys-18 of Pdx1. *c* and *d* show a larger region as in *a* and *b*, respectively, turned by 90°. In the structure of the ternary complex, Ser-75 and Asp-99 of Pdx1 (blue) mediate a reorganization of the substrate-binding region, including residues Glu-48, Arg-106, Asn-107, Asp-114, and Arg-135 of Pdx2. Observation of the ternary complex was facilitated by mutation of His-170 to Asn in Pdx2.

three-layered $\alpha\beta\alpha$ sandwich with Rossmann topology (10, 13, 14). An important functional segment in Pdx2 is the oxyanion region, between the so-called oxyanion strand β3 and helix α3 (Fig. 3, ochre). The peptide nitrogens of Gly-47 and Ala-80 are expected to form the oxyanion hole, an element necessary to stabilize the transient negative charge that occurs on the glutamine amide oxygen during catalysis (22, 23). The current high-resolution structure of Pdx2 at 1.7 Å (Table 2) reveals details not seen in the previously published 2.5-Å structure (13). In particular, Gly-47 is not correctly poised for oxyanion stabilization, because the peptide nitrogen is pointing away from the glutaminase active site (Fig. 3 *a* and *c*). In the ternary complex, interaction with αN of Pdx1 and the presence of glutamine induce a reorganization that leads to the formation of the oxyanion hole (Fig. 3 *b* and *d*). This conformation is stabilized by a reorientation of Gln-10, resulting in the loss of the hydrogen bond to the peptide nitrogen of Gly-47 and formation of a new hydrogen bond with the peptide carbonyl of Lys-18 in Pdx1 (Fig. 3 *a* and *b*). Concomitantly, the Gly-46/Gly-47 peptide undergoes a peptide flip, such that the peptide nitrogen of Gly-47 now points toward the amide oxygen of the substrate glutamine in the complex (compare Fig. 3 *c* and *d*). Thus, oxyanion hole formation is most likely a key regulatory step, analogous to that described for Ser and Cys proteases (24, 25). The conformation seen in the autonomous Pdx2 structure would then represent an enzymatic "ground state," similar to that observed for *Plasmodium falciparum* Pdx2 (14), as has also been observed in *Thermotoga maritima* ImGP (26), where the carbonyl oxygen points toward the substrate-binding site.

Aside from oxyanion hole formation, a number of changes surrounding the head group of bound glutamine occur in the ternary complex. Residues Glu-48, Arg-106, Asn-107, and Arg-135 in Pdx2 are seen in different orientations compared with the free enzyme, stabilized by interactions with the α2/β3 loop of Pdx1 (Fig. 3*d*). In particular, we observed that both the carbonyl and the side-chain hydroxyl group of Ser-75 in Pdx1 participate in hydrogen-bonding networks with residues around the active site of Pdx2, either directly or through water molecules. Furthermore, in all GATases examined so far, glutaminase and synthase activity is tightly coupled, mediated by binding of substrate in the synthase domain (21). Coupling has been observed for example in ImGP, and it has recently been proposed that it is mainly attributed to an interdomain salt bridge, which influences the precise alignment of catalytic residues in the active site of the glutaminase (21). This direct coupling, despite the observed structural divergence in synthase subunit architecture, was proposed to be a general feature of class I GATases. However, the recent biochemical characterization of PLP synthase has shown that the synthase substrates do not enhance the glutaminase half reaction (9). Moreover, we now observe that this specific interdomain contact is absent. Interestingly, though, the intramolecular salt bridge between Arg-135 and Asp-114 in autonomous Pdx2 is displaced by intermolecular salt bridges between R111, R135 of Pdx2, and Asp-99 of the α3/β4 loop of Pdx1 (Fig. 3 *c* and *d*). This contact may be of significance with respect to communication among the PLP synthase domains.

Discussion

Vitamin B_6 was discovered in the 1940s and has gained immense significance in the interim because of the vital role it plays in all organisms. As a consequence of the genomic era, it became clear only recently that the well studied *Escherichia coli* pathway is an exception, and most other organisms that synthesize the vitamin do so through an entirely different route (2, 7). In this context, the architecture of the synthesizing complex presented here is highly significant not only for knowledge of the machinery that synthesizes one of our essential nutrients but also for the development of potential antimicrobial or antiparasitic agents due to the absence of the pathway from animals (11, 14, 27, 28). Conversely, although the importance, ubiquity, and chemically distinct nature of GATases have been recognized, PLP synthase has properties clearly distinct from those of the canonical GATase and is the first reported GATase in such a higher oligomeric state (12). Furthermore, it displays a previously undescribed mode of interaction between glutaminase and synthase subunits, mediated by helix αN. Comparison with other class I GATases reveals that the presence of helix αN leads to an incongruent interaction between synthase and glutaminase subunits. PLP synthase and ImGP synthase (15, 16), for example, would require a rotation of 147° accompanied by a movement of 3.5 Å to match the glutaminase subunits of the two enzyme complexes, based on a superposition of the two synthase subunits (SI Fig. 7). Thus, the initial model (13) of the PLP synthase complex based on ImGP could not correctly predict the particular interface that is formed between Pdx1 and Pdx2. The importance of αN in Pdx1 is further emphasized by the crucial role it plays in controlling the activity of Pdx2, in that while directing the mode of interaction of both subunits, it covers the glutaminase active site, thus sequestering the substrate glutamine, and orchestrates glutaminase activation by triggering formation of the oxyanion hole, a prerequisite for catalysis. This phenomenon is clearly demonstrated through the availability of autonomous structures and that of the ternary complex.

PLP synthase is exceptional in that it catalyzes pentose and triose isomerizations, imine formation, amine addition, and ring formation, all in a single enzymatic system (8, 9). Two potential phosphate-binding sites that could be involved in substrate recognition are identified on the synthase subunit Pdx1, and they are referred to as P1 and P2 (Fig. 4*a*). In the structure of Pdx1, buffer component chloride ions were observed in these positions, whereas in PdxS (12), sulfate ions were found. P1 is on the C-terminal side of the $(\beta\alpha)_8$ barrel and comprises a characteristic loop apparently designed for phosphate binding (12) involving the amino acids Gly-

BIOCHEMISTRY

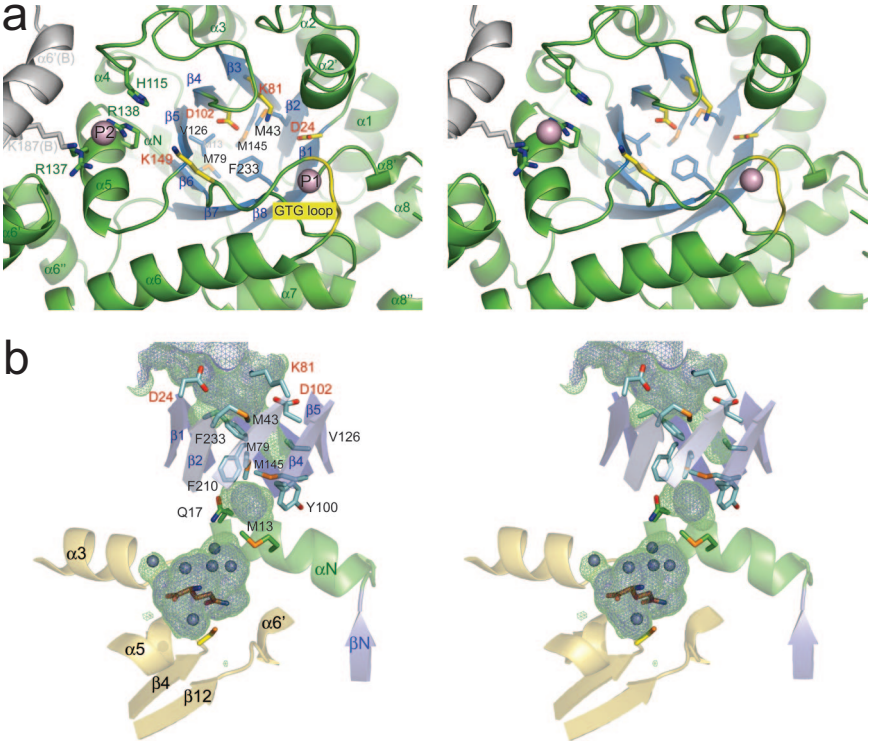

Fig. 4. Pdx1 active site and putative ammonia tunnel. (*a*) Buffer component Cl^- ions were observed in the sites marked as P1 and P2 in autonomous Pdx1. The binding site P1 at the C-terminal face of the barrel is characterized by a loop containing the amino acids Gly-Thr-Gly (GTG-loop in yellow) and is in close proximity to the catalytic center, consisting of D24 and K81. Residues H115, R137, and R138 from one subunit and K187 from an adjacent subunit form the P2-binding site. The catalytic residue Lys-149 is shown between P1 and P2. (*b*) Putative ammonia tunnel probed with a solvent radius of 1.2 Å (green) and 1.45 Å (blue). The cavity seen above the glutaminase active site is visible only in the ternary complex and is created by movement of Tyr-100 and Gln-17 of Pdx1 (compare Fig. 2*c*). A number of conserved hydrophobic residues line the proposed tunnel (M43, V126, M143, F210, and F233). In our model, we propose that the Mets in particular could change conformation to create a transient passage.

Thr-Gly (residues 153–155, GTG loop; yellow in Fig. 4*a*). Moreover, we have confirmed that residues Lys-81, Asp-24, and Asp-102, in the vicinity of P1, are necessary for catalysis, because mutation to Ala resulted in an enzyme without detectable PLP synthase activity (data not shown). These data together establish the Pdx1 active site around P1 on the catalytic face of the $(\beta\alpha)_8$-barrel, as is consistent with placement of active sites for all structurally known enzymes of this fold (18). Furthermore, it is interesting that residues 47–56, which form the small helical segment $\alpha2'$, are observed only in the ternary complex (Figs. 1*c* and 2*a*). This finding might indicate a "priming" of the synthase active site mediated by a signal from the glutaminase subunit.

The second site, P2, is at the interface of the hexameric rings. It is characterized by residues His-115, Arg-137, and Arg-138, in combination with Lys-187 from a second Pdx1 monomer (Fig. 4*a*). A shallow groove lined with charged residues connects P1 and P2 over a distance of 21 Å. Lys-149 (8, 12), at the center of this groove, is pointing toward P2, and by mutation to Ala, we confirmed its catalytic role, because the mutant protein is devoid of PLP synthesis activity (data not shown). The remoteness between glutaminase and synthase active sites raises the question of how the labile ammonia is transferred between them. An elegant way of how this can be accomplished is by channeling through the synthase domain. It has already been shown for ImGP that the core of a $(\beta\alpha)_8$-barrel can be used for the transfer of ammonia (15, 16, 33). However, a continuous channel could not be identified in the structure of either autonomous Pdx1 or the ternary complex. Indeed, one of the models proposed for the assembly of the PLP synthase complex was put forward on the basis that in the PdxS structure (12) no obvious channel could be observed, which in turn resulted in the erroneous prediction of adjacent active sites.

Comparative analysis of the 3D structures presented here allows us now to propose a model for ammonia transfer (Fig. 4*b*). First, as stated above, Gln-17 and Tyr-100 from the synthase subunit Pdx1 change their position in the ternary complex; αN is implied in organizing this structural switch (Fig. 2*c*). This movement creates a cavity inside the β-barrel, visible when probed with a solvent radius of 1.45 Å (Fig. 4*b*, blue map). It is plausible that this cavity is part of a passage/tunnel that could connect the two active sites over a distance of ≈22 Å. Among the hydrophobic residues in the core of the Pdx1 β-barrel, a number of Mets are observed (Fig. 4*b*). In this context, it has been documented that Met residues display a significant conformational plasticity [ref. 29; examples are the M domain of the signal recognition particle (30) or heat-shock proteins (31)]. Thus, we propose here that in Pdx1, consecutive movement of Met-13, -79, -145, and -43 (Fig. 4*b*) would allow ammonia to penetrate through the core of Pdx1. An additional cavity becomes visible, extending from the Pdx1 active site, when Pdx1 is probed with a solvent radius, of 1.2 Å (Fig. 4*b*, green map). This passage would have to widen to allow for passage of ammonia, requiring some plasticity of the surrounding residues [as is assumed to happen in the *E. coli* ammonium transporter with its narrow tunnel passage of only 0.6 Å (32)]. Ammonia would surface in close proximity to the catalytic residues Lys-81 and Asp-102 (Fig. 4). The discontinuity of the proposed channel in the current structure purports its transient nature, the opening of which is likely triggered by substrate binding. If the current proposal holds true, PLP synthase provides another example with a mechanism different from ImGP (15, 16, 33) for the transfer of ammonia, using the universal triosephosphate isomerase barrel fold (TIM). Although the presence of a transient tunnel in the core of the $(\beta\alpha)_8$-barrel might represent a destabilizing feature, the oligomeric state of Pdx1 could be an adequate ersatz, because oligomerization provides additional conformational stability (34).

Materials and Methods

Generation of Pdx1 and Pdx2 Constructs and Protein Expression and Purification. The constructs used in this study are described in ref. 9 and in SI *Supporting Text*. Expression and protein purification were carried out as described in ref. 9. Native Pdx2 was purified in a two-step protocol using a Source Q strong anion exchanger followed by gel filtration. For the PLP synthase complex, Pdx2-His_6 H170N and native Pdx1 were coexpressed in *E. coli* BL21 (DE3) cells (Stratagene, La Jolla, CA). Purification was carried out using

a two-step protocol of Ni-affinity chromatography and gel filtration in the presence of 10 mM glutamine. Complete information on purification of all proteins is in SI *Supporting Text*.

Biochemical and Biophysical Protein Assays. The glutaminase activity assay was performed as described in ref. 9 using a 4 μM concentration of either the wild-type or mutated Pdx1 and Pdx2 proteins. PLP synthase activity was also determined as described in ref. 9, with the exception that 20 μM each of the proteins was used and 0.5 mM ribose-5-phosphate and 1.0 mM DL-glyceraldehyde-3-phosphate were used as substrates. For native PAGE mobility-shift assays, equimolar concentrations of the respective Pdx1 and Pdx2 proteins were preincubated in the presence of glutamine (10 mM) for 15 min at 37°C followed by electrophoresis in 12.5% gels. Western blot analysis was performed as described in ref. 9.

The association states of Pdx1 and Pdx1/2 complexes in solution were determined by hydrodynamic analysis in analytical ultracentrifugation experiments using a Beckman Optima XL-A ultracentrifuge equipped with absorbance optics and an An60 Ti rotor (Beckman Coulter, Fullerton, CA). Sedimentation velocity studies were carried out at 35,000 rpm at 20°C using protein with an absorbance at 280 nm of 1. Partial specific volumes $\bar{v}$, extinction coefficients at 280 nm, buffer density ρ, and viscosity η were calculated by using the program SEDNTERP, Version 1.05 (J. Philo, D. Hayes, and T. Laue, www.jphilo.mailway.com/download.htm). Calculated partial specific volumes $\bar{v}$ for both Pdx2 and Pdx1 are 0.742 ml·g^{-1}; the calculated extinction coefficient is 10,930 M^{-1}·cm^{-1} for Pdx1 and 2,980 M^{-1}·cm^{-1} for Pdx2. Centrifugation was conducted in 20 mM Tris·Cl, pH 7.5, and 200 mM KCl with ρ = 1.0084 g·ml^{-1} and η = 1.0045 mPa for WT Pdx1 and in 20 mM Tris·Cl, pH 8.0, and 300 mM KCl with ρ = 1.01291 g·ml^{-1} and η = 1.0031 mPa for Pdx1 Δ1–18 and Pdx1/2 complexes. Theoretical hydrodynamic parameters were determined from the crystal structure coordinates by creating models composed of spherical beads of varying size with the program HYDROPRO on a Linux-PC using the subroutine Hydropro5amsd (35). The hexamer–dodecamer equilibrium was fitted to the velocity data according to

$$2(\mathrm{Pdx1})_6 \underset{k_{-1}}{\overset{k_1}{\rightleftharpoons}} (\mathrm{Pdx1})_{12} \qquad [1]$$

X-Ray Crystallographic Structure Determination. The three 3D structures determined in this study were crystallized by using hanging-drop vapor diffusion experiments. Crystals were flash-frozen by using ethylene glycol as cryoprotectant. Data were collected at 100°K at the European Synchrotron Radiation Facility in Grenoble, France, and integrated and scaled with the HKL software (36). All additional data manipulation was carried out with the CCP4 suite of programs (37). The structures were determined by molecular replacement by using the program MOLREP (38) with the coordinate sets of 1ZNN (12) for Pdx1 and of 1R9G (13) for Pdx2. Iterative model building and refinement were carried out with the programs O (39) and REFMAC5 (40) cycled with ARP (41), using TLS refinement in the final cycles. Large crystals of up to $1 \times 0.2 \times 0.2$ mm^3 could be grown from Pdx2 at a concentration of $\approx$20 mg·ml^{-1} using 12.4% PEG 8000/6% ethylene glycol/100 mM cacodylic acid, pH 6.2, as crystallization buffer. Pdx1-His$_6$ was concentrated to $\approx$20 mg·ml^{-1} for crystallization in 100 mM Tris·Cl, pH 7.8/15–20% ethanol/200 mM $MgCl_2$. Hexagon-shaped disks of a size of $150 \times 150 \times 30$ μm^3 diffracted to 2.6 Å. Orthorhombic crystals occasionally grew under the same conditions and diffracted to 2.2 Å. A Pdx1 dodecamer extends over two crystallographic asymmetric units, with the crystallographic twofold relating two hexamers. The Pdx1:Pdx2 H170N:glutamine ternary complex was concentrated to $\approx$24 mg·ml^{-1} for crystallization in 15–17% PEG 4000 buffered with 200 mM triammonium citrate at pH 7.0. Plate-like crystals of a size of $100 \times 200 \times 50$ μm^3 diffracted to 2.1 Å. After rigid-body refinement of the initial molecular replacement solution using Pdx1 electron-density maps showed the position and orientation of Pdx2 molecules, and these were docked manually by using O (39). All structural diagrams were drawn by using PyMOL (ref. 42; www.pymol.org).

Note Added in Proof. While this manuscript was in press, we learned that the x-ray structure of PLP synthase from *T. maritima* has been accepted for publication (43).

We thank the European Synchrotron Radiation Facility for access to beamlines ID14–1, ID23, and ID29; the beamline staff for support during data collection; and Gordon Leonhard for additional beamtime allocation. We thank Prof. Nikolaus Amrhein for helpful discussions. T.B.F. thanks the Swiss National Science Foundation (SNF) (Grant 3100A0–107975/1) for generous support to both her and Prof. Nikolaus Amrhein. Marina Tambasco-Studart (Eidgenössiche Technische Hochschule Zürich) is thanked for performing the H170N mutation of Pdx2. We thank Sabine Kaltofen for experimental support. T.B.F. and I.T. acknowledge support by the European Commission (Grant VITBIOMAL-012158). We also thank the members of this consortium for constructive discussions, in particular Dr. Barbara Kappes, who initiated VITBIOMAL.

1. Bender DA (1989) *Eur J Clin Nutr* 43:289–309.
2. Ehrenshaft M, Bilski P, Li MY, Chignell CF, Daub ME (1999) *Proc Natl Acad Sci USA* 96:9374–9378.
3. Tambasco-Studart M, Titiz O, Raschle T, Forster G, Amrhein N, Fitzpatrick TB (2005) *Proc Natl Acad Sci USA* 102:13687–13692.
4. Cane DE, Du S, Robinson JK, Hsiung Y, Spenser ID (1999) *J Am Chem Soc* 121:7722–7723.
5. Laber B, Maurer W, Scharf S, Stepusin K, Schmidt FS (1999) *FEBS Lett* 449:45–48.
6. Mittenhuber G (2001) *J Mol Microbiol Biotechnol* 3:1–20.
7. Osmani AH, May GS, Osmani SA (1999) *J Biol Chem* 274:23565–23569.
8. Burns KE, Xiang Y, Kinsland CL, McLafferty FW, Begley TP (2005) *J Am Chem Soc* 127:3682–3683.
9. Raschle T, Amrhein N, Fitzpatrick TB (2005) *J Biol Chem* 280:32291–32300.
10. Zalkin H, Smith JL (1998) *Adv Enzymol Relat Areas Mol Biol* 72:87–144.
11. Sakai A, Kita M, Tani Y (2004) *J Nutr Sci Vitaminol (Tokyo)* 50:69–77.
12. Zhu J, Burgner JW, Harms E, Belitsky BR, Smith JL (2005) *J Biol Chem* 280:27914–27923.
13. Bauer JA, Bennett EM, Begley TP, Ealick SE (2004) *J Biol Chem* 279:2704–2711.
14. Gengenbacher M, Fitzpatrick TB, Raschle T, Flicker K, Sinning I, Muller S, Macheroux P, Tews I, Kappes B (2006) *J Biol Chem* 281:3633–3641.
15. Chaudhuri BN, Lange SC, Myers RS, Chittur SV, Davisson VJ, Smith JL (2001) *Structure (Cambridge, UK)* 9:987–997.
16. Douangamath A, Walker M, Beismann-Dreimeyer S, Vega-Fernandez MC, Sterner R, Wilmanns M (2002) *Structure (Cambridge, UK)* 10:185–193.
17. Amuro N, Paluh JL, Zalkin H (1985) *J Biol Chem* 260:14844–14849.
18. Sterner R, Hocker B (2005) *Chem Rev* 105:4038–4055.
19. Dam J, Schuck P (2004) *Methods Enzymol* 384:185–212.
20. Brown PH, Schuck P (2006) *Biophys J* 90:4651–4661.
21. Myers RS, Amaro RE, Luthey-Schulten ZA, Davisson VJ (2005) *Biochemistry* 44:11974–11985.
22. Chittur SV, Klem TJ, Shafer CM, Davisson VJ (2001) *Biochemistry* 40:876–887.
23. Chaudhuri BN, Lange SC, Myers RS, Davisson VJ, Smith JL (2003) *Biochemistry* 42:7003–7012.
24. Menard R, Storer AC (1992) *Biol Chem Hoppe-Seyler* 373:393–400.
25. Barrette-Ng IH, Ng KK, Mark BL, Van Aken D, Cherney MM, Garen C, Kolodenko Y, Gorbalenya AE, Snijder EJ, James MN (2002) *J Biol Chem* 277:39960–39966.
26. Korolev S, Skarina T, Evdokimova E, Beasley S, Edwards A, Joachimiak A, Savchenko A (2002) *Proteins* 49:420–422.
27. Cassera MB, Gozzo FC, D'Alexandri FL, Merino EF, del Portillo HA, Peres VJ, Almeida IC, Eberlin MN, Wunderlich G, Wiesner J, *et al*. (2004) *J Biol Chem* 279:51749–51759.
28. Wrenger C, Eschbach ML, Muller IB, Warnecke D, Walter RD (2005) *J Biol Chem* 280:5242–5248.
29. Gellman SH (1991) *Biochemistry* 30:6633–6636.
30. Keenan RJ, Freymann DM, Walter P, Stroud RM (1998) *Cell* 94:181–191.
31. Sundby C, Harndahl U, Gustavsson N, Ahrman E, Murphy DJ (2005) *Biochim Biophys Acta* 1703:191–202.
32. Khademi S, O'Connell J, 3rd, Remis J, Robles-Colmenares Y, Miercke LJ, Stroud RM (2004) *Science* 305:1587–1594.
33. Amaro RE, Myers RS, Davisson VJ, Luthey-Schulten ZA (2005) *Biophys J* 89:475–487.
34. Neet KE, Timm DE (1994) *Protein Sci* 3:2167–2174.
35. Garcia De La Torre J, Huertas ML, Carrasco B (2000) *Biophys J* 78:719–730.
36. Otwinowski Z, Minor W (1997) *Methods Enzymol* 276:307–326.
37. Collaborative Computational Project, Number 4 (1994) *Acta Crystallogr D* 50:760–763.
38. Vagin AA, Teplyakov A (1997) *J Appl Crystallogr* 30:1022–1025.
39. Jones TA, Zou JY, Cowan SW, Kjeldgaard M (1991) *Acta Crystallogr A* 47:110–119.
40. Murshudov GN, Vagin AA, Dodson EJ (1998) *Acta Crystallogr D* 54:905–921.
41. Lamzin VS, Wilson KS (1997) *Methods Enzymol* 277:269–305.
42. DeLano WL (2002) *The PyMOL Molecular Graphics System* (DeLano Scientific, San Carlos, CA).
43. Zein F, Zhang Y, Kang YN, Burns K, Begley TP, Ealick SE (2006) *Biochemistry*, in press.

Structure of a bacterial pyridoxal 5'-phosphate synthase complex

— Supporting Information —

Marco Strohmeier[*,§], Thomas Raschle [†,§], Jacek Mazurkiewicz[‡], Karsten Rippe[‡], Irmgard Sinning[*], Teresa B. Fitzpatrick[†,¶] and Ivo Tews[*,¶]

* Heidelberg University Biochemistry Center, Im Neuenheimer Feld 328, D-69120 Heidelberg, Germany. † ETH Zurich, Institute of Plant Sciences, Universitätstrasse 2, 8092 Zurich, Switzerland. ‡ Molecular Biophysics Group, Kirchhoff Institute for Physics, Heidelberg University, Im Neuenheimer Feld 227, D-69120 Heidelberg, Germany.

§ These authors contributed equally to the work

¶ To whom correspondence should be addressed. E-mail: teresa.fitzpatrick@ipw.biol.ethz.ch & ivo.tews@bzh.uni-heidelberg.de.

Supporting Information includes:

Materials and Methods

Generation of Pdx1 and Pdx2 constructs. The constructs pET*Bs*Pdx1, pET*Bs*Pdx2 and pET*Bs*Pdx2-His_6 described in 1 were used in this study. pET*Bs*Pdx1-His_6 was constructed using genomic DNA as template and the primers 5' primer: CTAGCTAGCATGGCTCAAACAGGTACTGAACG and 3' primer: CCGCTCGAGCCAGCCGCGTTCTTGCATACGC for amplification, followed by cloning into the NheI/XhoI restriction sites of pET21a (EMD Biosciences, Inc., Novagen Brand, Madison, WI, USA). pETΔN1-18*Bs*Pdx1, the N-terminal truncated version of Pdx1 missing the first 18 amino acids (Pdx1 Δ1-18), was constructed using the 5' primer CTAGCTAGCATGGGCGGCGTCATCATGGACGTC and the 3' primer CCGCTCGAGCCAGCCGCGTTCTTGCATACGC to amplify the DNA while using pET*Bs*Pdx1 as the template. The fragment was cloned into the NheI/XhoI restriction sites of pET21a (EMD Biosciences, Inc., Novagen Brand, Madison, WI, USA). Cloning into the vector in this way allows expression of the protein(s) with a C-terminal hexa-histidine affinity tag. Mutagenesis was carried out using the QuikChange site-directed mutagenesis (Stratagene, La Jolla, CA, USA) according to the manufacturer's instructions. The following oligonucleotides were used to change the desired codon: Pdx2 H170N, 5' primer CCTTGGCTGCTCATTCAATCCGGAGCTGACA and 3' primer: CTGTCAGCTCCGGATTGAATGAGCAGCCAAGG using pET*Bs*Pdx2 as the template (9); Pdx1 D24A, 5' primer: GGCGGCGTCATCATGGCCGTCATCAATGCGGAA and 3' primer: TTCCGCATTGATGACGGCCATGATGACGCCGCC; Pdx1 K81A, 5' primer:

CCCGGTAATGGCAGCAGCGCGTATCGG and 3' primer: CCGATACGCGCTGCTGCCATTACCGGG; Pdx1 K149A, 5' primer: GCTTCGCACTGCAGGTGAGCCTGG and 3' primer: CCAGGCTCACCTGCAGTGCGAAGC using pET*Bs*Pdx1 as the template.

Protein expression and purification. Expression of all proteins was carried out as described in (1). For purification, bacteria were resuspended in lysis buffer and lysed by cell disruption using a fixed geometry fluid processor (Microfluidics Corporation, Newton, MA, USA), followed by clarification through ultracentrifugation (170,000 g, 20 minutes, 4 °C). Native Pdx2 was purified in a two-step protocol using a Source Q strong anion exchanger followed by gel filtration on a S75 (26/60) column (both GE Healthcare, Easton Turnpike Fairfield, CT, USA). Buffers were as follows: lysis buffer, 50 mM Tris-Cl pH 7.3, 10 mM NaCl, 0.4 mM DTT, 1 mM EDTA, 1.2 mM PMSF and 10% glycerol; Source Q-buffer: as for lysis buffer, but using a continuous gradient of 0-1 M NaCl for elution; Gel filtration buffer: 20 mM Tris-Cl pH 6.8, 200 mM KCl and 0.02% monothioglycerol (MTG). Hexahistidine tagged Pdx2 (Pdx2-His_6) and Pdx2 H170N ware purified as described in (1). Hexahistidine tagged Pdx1 (Pdx1-His_6) and mutant proteins Pdx1 Δ1-18, Pdx1 D24A, Pdx1 K81A and Pdx1 K149A were purified in a two-step protocol using Ni-affinity chromatography and gel-filtration on a S200 (26/60) column (both GE Healthcare, Easton Turnpike Fairfield, CT, USA). Lysis buffer: 50 mM NaH_2PO_4 pH 8, 300 mM NaCl and 10 mM imidazole; elution buffer: as for lysis buffer, but with 0.3 M imidazole; Gel filtration buffer: 20 mM Tris-Cl pH 6.8, 200 mM KCl and 0.02% MTG. Native Pdx1 was

purified as described in (1), followed by gel-filtration as described for Pdx1-His_6. For the purification of the PLP synthase complex, Pdx2-His_6 H170N and native Pdx1 were co-expressed in *E. coli* BL21 (DE3) cells (Stratagene, La Jolla, CA, USA). Purification was carried out using Ni-affinity chromatography as described above for Pdx1-His_6 followed by gel filtration on a Superose 6 (10/30) column (both GE Healthcare, Easton Turnpike Fairfield, CT, USA) equilibrated in 20 mM Tris-Cl pH 8, 300 mM KCl and 0.02% MTG in the presence or absence of 10 mM glutamine.

TABLES

Table 2 Data collection and refinement statistics

	Pdx2 native	Pdx1 native	Pdx1:Pdx2:glutamine
Symmetry	$P2_12_12_1$	$P2_12_12$	$P2_1$
Unit cell a x b x c ($Å^3$) beta angle	45.4 x 81.6 x 117.3	101.1 x 106.2 x 182.3	93.6 x 259.2 x 145.1 92.15°
Solvent content (%)	42.9	41.3	45.9
# mol in AU	2	6	12 x Pdx1 12 x Pdx2
Average B ($Å^2$)	28	25	29
Unique reflections	45,697	116,594	381,798
Mosaicity (°)	0.60	0.51	0.31
Resolution / HR shell (Å)	50-1.73 / 1.75-1.73	50-2.08 / 2.10-2.08	50-2.12 / 2.14-2.12

R_{sym} / HR shell (%)*	6.5 / 49.2	10.3 / 47.9	8.1 / 49.5
Completeness / HR shell (%)	98.4 / 99.9	98.6 / 98.1	98.2 / 98.4
I / sigI / HR shell	17.3 / 2.0	9.0 / 2.1	12.0 / 2.2
Redundancy / HR shell	5.3 / 3.9	3.2 / 3.3	3.1 / 3.1
Refinement statistics			
Amino acids	384	1,529	5,568
Total protein atoms (including double conformations)	3,012	11,416	42,000
Waters	451	1,748	5,646
Ligands atoms	none	140 11 ethylene glycol 12 Cl^- 12 Mg^{2+}*6 H_2O	192 12 x Glutamine 15 ethylene glycol 12 Cl^-
RMSD bond (Å)	0.022	0.023	0.018
RMSD angle (°)	1.96	1.87	1.73
R_{free} (%)‡	22.9	19.3	20.5
R_{work} (%)†	18.4	14.4	15.4

*$R_{sym} = \Sigma_h\Sigma_i |I(h) - I(h)_i|/\Sigma_h\Sigma_i I(h)_i$, where I(h) is the mean intensity after rejections

†$R_{work} = \Sigma_h||F_{obs}(h)| - |F_{calc}(h)||/ \Sigma h|F_{obs}(h)|$, where $F_{obs}(h)$ and $F_{calc}(h)$ are observed and calculated structure factors, respectively

‡5% of the data were excluded to calculate R_{free}

FIGURE LEGENDS

Fig. 5. Scheme depicting the complex assembly. The ribbon diagrams are shown in two orientations, turned by 90°. Labeling indicates whether the particular assembly is hypothetical, an observed 3D-structure, or observed in solution. When analytical ultracentrifugation data were available (compare Table 1), calculated as well as experimental sedimentation coefficients are given (calc. and exp. sed. coeff., respectively). (*a*) A single Pdx1 subunit, which has a classic $(\beta\alpha)_8$-barrel fold, with two significant alterations to the regular structure. Firstly, helix α8' is inserted after helix α8. Secondly, helix α6 is elongated and followed by two inserted helical segments, helix α6' and α6". (*b*) The Pdx1 hexamer. Helix α8' is at the interface of adjacent monomers in the hexameric ring. (*c*) The Pdx1 dodecamer. The elongated helix α6 and the inserted helices α6' and α6" form dents that interdigitate when two hexamers form the dodecamer. (*d*) Pdx1 dodecamer with a single Pdx2 subunit attached. Binding of Pdx2 orders the N-terminal helix, αN, of Pdx1 and allows for formation of a β-strand, βN, at the very N-terminus of Pdx1 which forms a β-sheet with β7 and β8 of Pdx2. The helical segment α2' is only seen in the complex between Pdx2 and Pdx1. (*e*) The fully occupied complex between Pdx1, Pdx2 H170N and substrate glutamine. The two Pdx1 hexameric rings are distinguished by two shades of green with one Pdx1 monomer shown in blue, Pdx2 is shown in orange with one monomer highlighted in red.

Fig. 6. Analysis of complex formation by sedimentation velocity ultracentrifugation. In panels (*a*) and (*b*) the distributions of sedimentation coefficients are shown, s-values given are corrected to standard conditions ($s_{20,w}$ for 20 °C, H_2O). To facilitate comparison, data in the two graphs were scaled to the same maximum value. (*a*) (…) Autonomous Pdx1 is in a hexamer-dodecamer equilibrium with average sedimentation coefficients of 8.7 ± 0.3 S for $(Pdx1)_6$ and 13.7 ± 0.3 S for $(Pdx1)_{12}$. (·-·-) Pdx1 and Pdx2 H170N in the presence of glutamine. The sedimentation coefficient (17.2 ± 0.8) represents a $(Pdx1)_{12}$-$(Pdx2)_{12}$ complex. (*b*) (—) In the absence of glutamine, the $(Pdx1)_{12}$-$(Pdx2)_{12}$ complex is not fully formed with a sedimentation coefficent 15.7 ± 0.9 S). (- - -) Addition of glutamine leads to the cooperative formation of a $(Pdx1)_{12}$-$(Pdx2)_{12}$ complex with a sedimentation coefficient of 17.5 ± 0.4 S. (…) Pdx1 Δ1-18 is unable to complex with Pdx2; peaks at sedimentation values of 13.3 ± 0.9 S and 8.3 ± 0.9 S represent the hexameric and dodecameric species of the autonomous synthase subunit, compare panel (*a*). (*c*) Sedimentation velocity ultracentrifugation of Pdx1 fitted to a hexamer-dodecamer equilibrium. The bottom panel shows the experimental data and the fitted curves as a function of the radial position. On the top, the residuals of the fits are plotted. The molecular mass of the hexamer was fixed at the theoretical value of 189 kDa. Only every third scan is shown.

Fig. 7. Comparison of the structures of (*a*) PLP- and (*b*) ImGP synthase. The orientation of ImGP synthase is as in (2). For PLP synthase, the orientation of the synthase subunit that forms a $(\beta\alpha)_8$ barrel is as in ImGP synthase, which reveals that the presence of helix αN in PLP synthase leads to a different interaction that offsets the glutaminase domain at the

bottom by 147° with a concomitant movement of 3.5 Å. Color coding has been adapted from Fig. 2. For the glutaminase, the central β-sheet is colored in red to show the orientation of the molecule. For the synthase, helices αN and α2' are shown in green.

REFERENCES

1 Raschle, T., Amrhein, N. & Fitzpatrick, T.B. (2005) *J. Biol. Chem.* **280**, 32291-32300.

2 Bauer, J.A., Bennett, E.M., Begley, T.P. & Ealick, S.E (2004). *J. Biol. Chem.* **279**, 2704-2711.

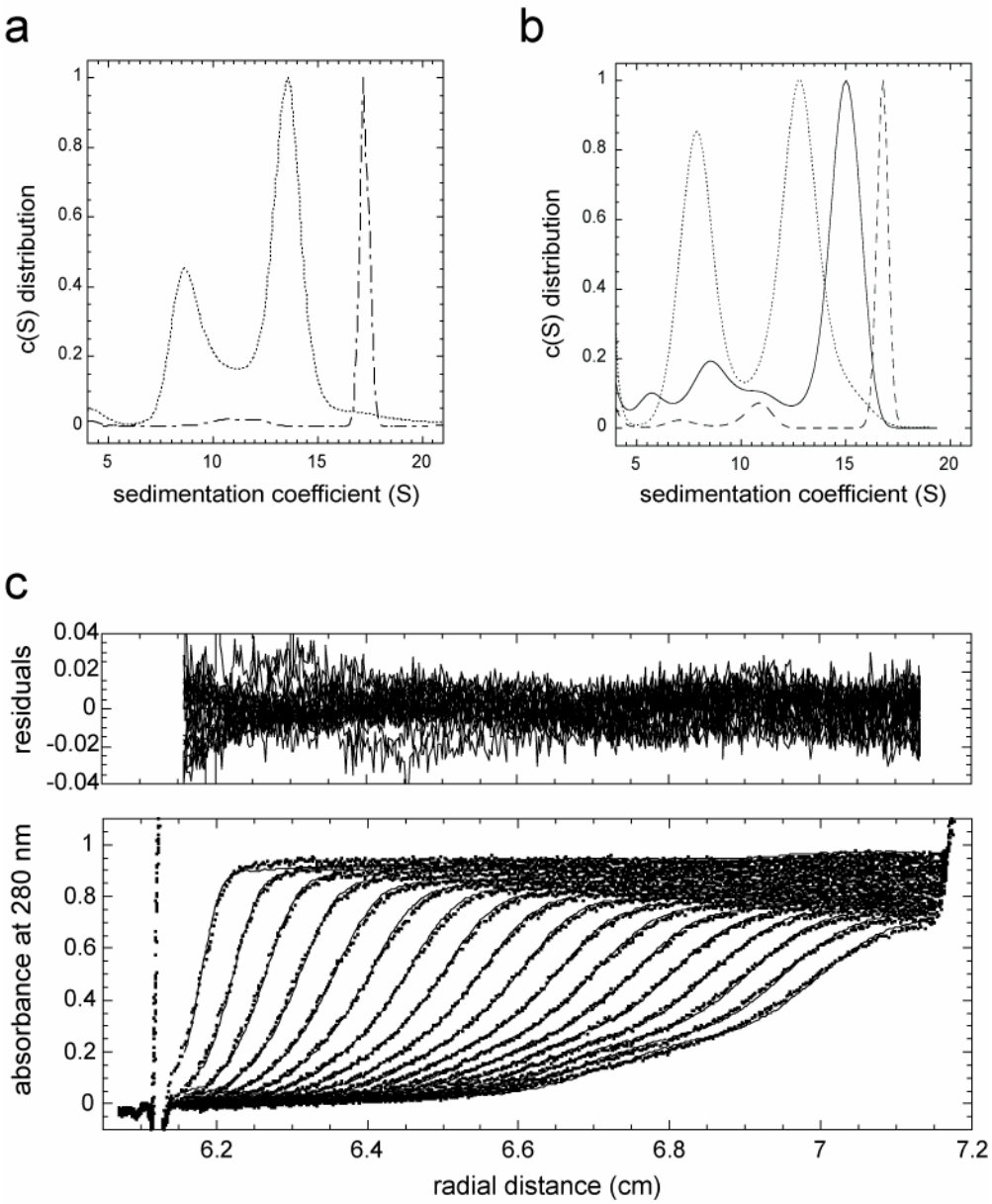

Strohmeier *et al.*, Figure 6

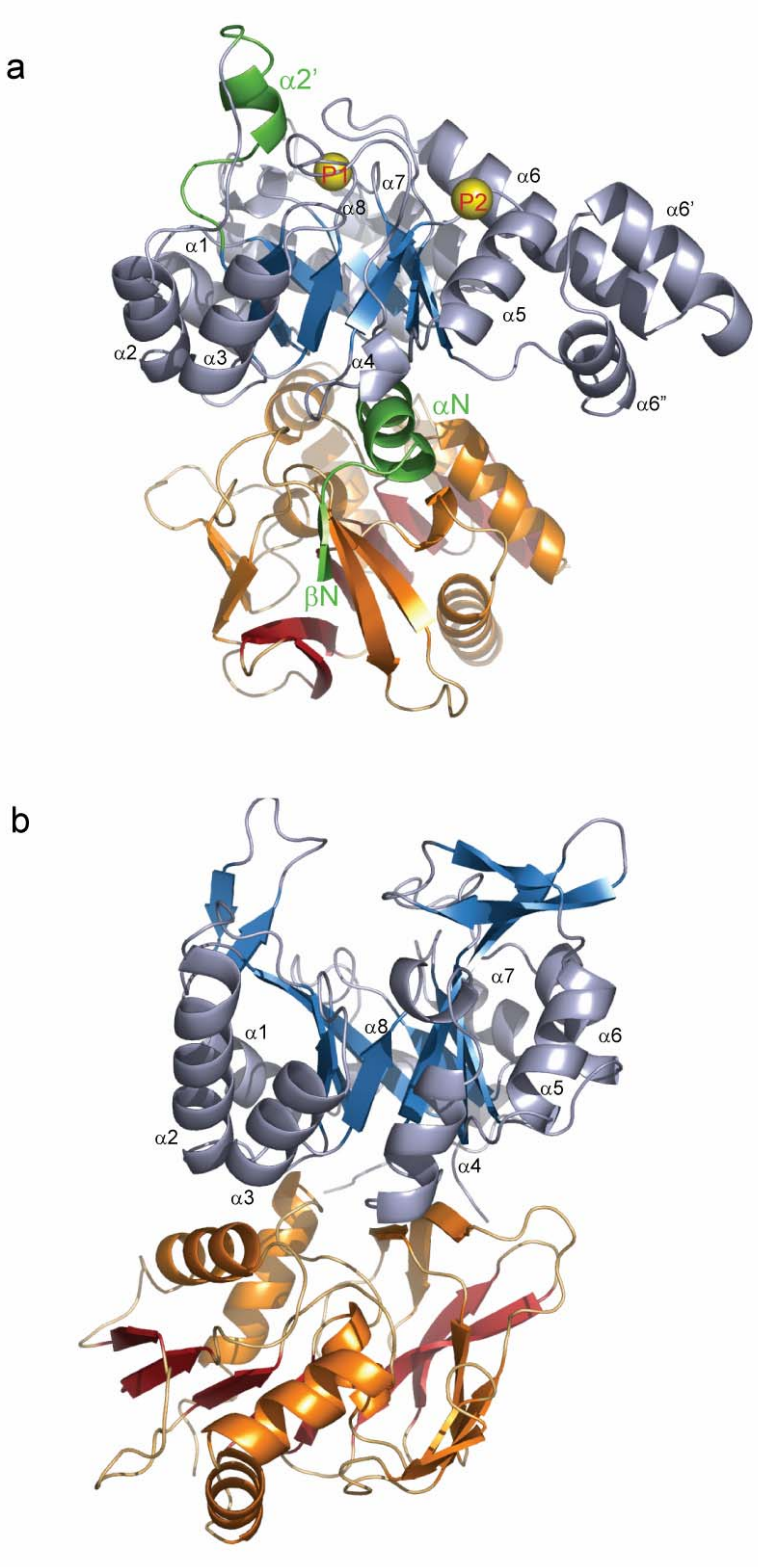

Strohmeier *et al.*, Figure 7

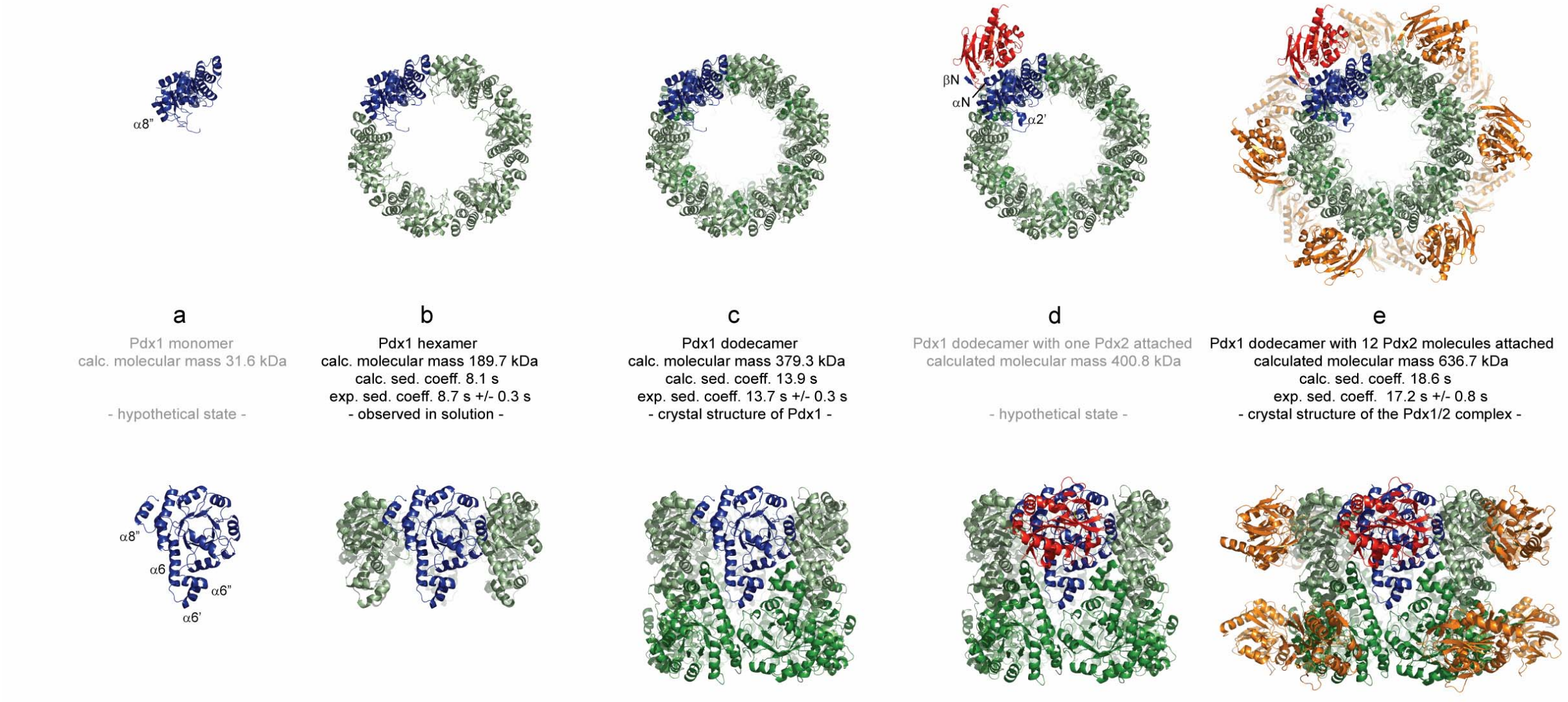

Strohmeier *et al.*, Figure 5